metals MDPI

Article

Design of Novel Flash Ironmaking Reactors for Greatly Reduced Energy Consumption and CO_2 Emissions

Hong Yong Sohn *, De-Qiu Fan and Amr Abdelghany †

Department of Materials Science & Engineering, University of Utah, Salt Lake City, UT 84112-0114, USA; jerrydqfan@gmail.com (D.-Q.F.); amr.abdelghany@eng1.cu.edu.eg (A.A.)
* Correspondence: h.y.sohn@utah.edu; Tel.: +1-801-581-5491
† Current address: Chemical Engineering Department, Faculty of Engineering, Cairo University, Giza 12613, Egypt.

Abstract: The development of a novel ironmaking technology based on fine iron ore concentrate in a flash reactor is summarized. The design of potential industrial reactors for flash ironmaking based on the computational fluid dynamics technique is described. Overall, this simulation work has shown that the size of the reactor used in the novel flash ironmaking technology (FIT) can be quite reasonable vis-à-vis the blast furnaces. A flash reactor of 12 m diameter and 35 m height with a single burner operating at atmospheric pressure would produce 1.0 million tons of iron per year. The height can be further reduced by either using multiple burners, preheating the feed gas, or both. The computational fluid dynamics (CFD)-based design of potential industrial reactors for flash ironmaking pointed to a number of features that should be incorporated. The flow field should be designed in such a way that a larger portion of the reactor is used for the reduction reaction but at the same time excessive collision of particles with the wall must be avoided. Further, a large diameter-to-height ratio that still allows a high reduction degree should be used from the viewpoint of decreased heat loss. This may require the incorporation of multiple burners and solid feeding ports.

Keywords: concentrate; flash ironmaking technology (FIT); hydrogen; kinetics; magnetite; natural gas; CFD simulation; reactor design; partial combustion

Citation: Sohn, H.Y.; Fan, D.-Q.; Abdelghany, A. Design of Novel Flash Ironmaking Reactors for Greatly Reduced Energy Consumption and CO_2 Emissions. *Metals* **2021**, *11*, 332. https://doi.org/10.3390/met11020332

Academic Editor: Henrik Saxen

Received: 15 January 2021
Accepted: 7 February 2021
Published: 14 February 2021

1. Introduction

Ironmaking consumes large amounts of energy and produces a great deal of carbon dioxide. Therefore, a critical problem facing the steel industry is the development of an innovative technology for producing iron that is much more energy-efficient and environmentally friendly. It should also be much less expensive than the blast furnace/coke oven combination, and must be capable of producing iron at a sufficiently large rate to feed steel mills. This article describes the development of a novel flash ironmaking technology (FIT), conceived by Sohn [1], which is based on the reduction of iron oxide concentrate particles by gaseous fuel/reductant in a vertical flash reactor. The novel process addresses the critical issues in ironmaking, namely, energy saving and greenhouse-gas emissions. The steel industry is responsible for about 6–7% of total human-made emissions of carbon dioxide [2].

The solid feed in the currently dominant blast furnace process is iron ore sinters or pellets and coke made from coking coal, the production of both which uses a great deal of energy and is prone to environmental pollution. The alternative ironmaking direct reduction processes [3] are divided into two different categories: shaft furnace processes (Midrex and Energiron [4]) and fluidized-bed processes (e.g., FIOR [5], FINMET [5], CIRCORED [6], and SPIREX [7]). These processes, however, are not intensive enough to compete with the blast furnace. The shaft furnace processes must use pellets of iron oxide concentrate that consume energy and emit pollutants including CO_2 during production.

A novel flash ironmaking technology (FIT) has been conceived by Sohn [1] for producing iron directly from fine concentrates by a flash reduction process. This process uses a reductant gas such as natural gas, hydrogen, or a mixture of the two, does not require pellets, sinters or coke as required by other ironmaking processes [1,8–10]. The new technology would significantly reduce energy consumption by 30–60% and decrease carbon dioxide emissions by 60–96% compared with blast furnace ironmaking, depending on whether hydrogen or hydrocarbon gas is used. The FIT will not have problems like particles sticking or pellet disintegration. High-grade lump iron ore is scarce world-side, and new reserves must be ground to finer sizes to beneficiate them. Thus, increasing amounts of concentrates that can feed the FIT reactor are expected to be produced world-wide [11].

Based on the potential advantages discussed here and the results of the process feasibility studies, detailed flow sheets for different versions of the new process depending on the fuel type and economic analysis have been developed by Pinegar et al. [12–15].

Articles on the description of flash ironmaking and comparison with other processes together with review of the literature have been published previously [8,9,12,13]. This article focuses on the design of flash reactors based on computational fluid dynamics (CFD) simulation and modeling.

2. Description of Flash Ironmaking Technology (FIT)

A sketch of the new flash ironmaking process is shown in Figure 1. In this process, the fuel gas is partially burned with tonnage oxygen, which generates a reducing gas of 1500–1800 K. The injected concentrate particles are reduced as they move downward. The process may be operated to create a molten-iron bath for possible direct steelmaking or to produce solid iron particles that can be charged in subsequent steelmaking furnaces.

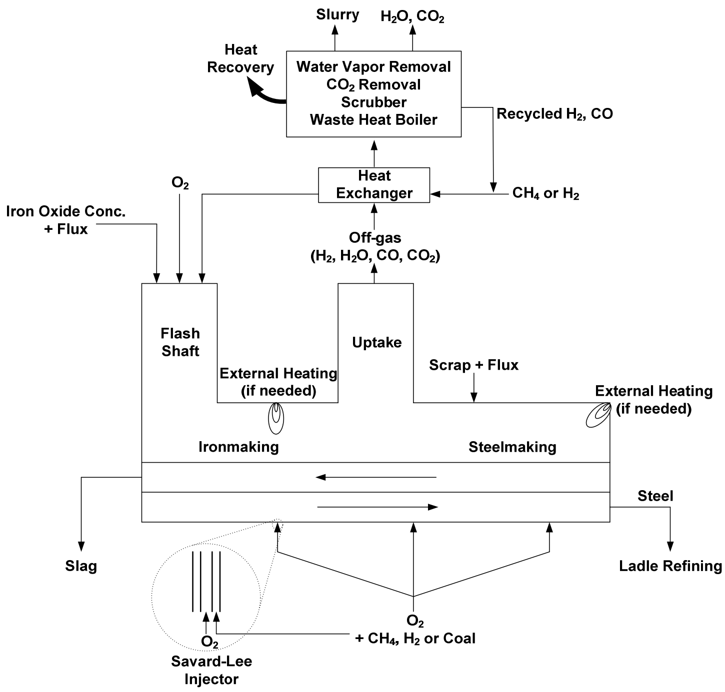

Figure 1. A schematic diagram of a possible direct steelmaking process based on flash ironmaking technology (FIT).

The flash ironmaking technology (FIT) is expected to eliminate several of the critical issues accompanying other alternate ironmaking processes such as (a) the requirements of pelletization or sintering, (b) cokemaking, (c) solids sticking or disintegration, and (d) refractory erosion. This technology offers the possibility to produce either solid iron particles or molten iron that leads to direct steelmaking in a single unit, as shown in Figure 1.

3. Reduction Kinetics of Magnetite Concentrate Particles

Hydrogen is the main reducing agent in the new process that takes place at temperatures above 1473 K, even when an H_2 + CO mixture produced by the partial combustion of natural gas is used. Carbon monoxide is highly stable at these high temperatures and thus its direct contribution is much less from the viewpoints of thermodynamics and also kinetics relative to hydrogen. However, it provides a synergistic effect on the hydrogen reduction, as shown below. Sohn and coworkers [16–21] have investigated the reduction rates of magnetite and hematite concentrates under the temperature ranges and gaseous reactant partial pressures applicable to the flash ironmaking technology (FIT), using laminar-flow reactors. The results were found to yield rate equations that can be expressed by the following general form of $\frac{dX}{dt}$ for both component gases H_2 and CO:

$$\left.\frac{dX}{dt}\right|_j = k_j\left(p_j^{m_j} - \left(\frac{p_{jO}}{K_j}\right)^{m_j}\right)n_j\,(1-X)(-Ln(1-X))^{1-1/n_j}d_p^{-s_j};\ j = \mathrm{H_2 \text{ or } CO} \quad (1)$$

where k_j is the reaction rate constant for gas j, $k_j = k_{o,j}\exp\left(-\frac{E_j}{RT}\right)$; p_j is the partial pressure of gas j; K_j is the equilibrium constant for the reduction of FeO by gas j; m_j is the reaction order with respect to gas j; n_j is the Avrami parameter; $d_p^{-s_j}$ is the particle size effect function; and X is the reduction degree defined as the ratio of the removed oxygen to the total removable oxygen in the concentrate particles.

The rate parameters that are most appropriate for application in designing and analyzing the operation of a flash ironmaking reactor are given below. The reader is referred to the original papers for other details of the rate measurement and data analysis.

Table 1 lists the kinetic parameters for the reduction of magnetite concentrate by individual component gases.

Table 1. Kinetic parameters for reduction of magnetite concentrate by individual component gases [16,17,20,21].

Reducing Gas, j	Temperature Range	$k_{o,j}$	E_j (kJ/mol)	m_j	n_j	s_j
H_2	1423–1623 K	1.23×10^7 atm$^{-1}\cdot$s^{-1}	196	1	1	0
	1623–1873 K	6.07×10^7 atm$^{-1}\cdot$s$^{-1}\cdot$µm	180	1	1	1
CO	1423–1623 K	1.07×10^{14} atm$^{-1}\cdot$s^{-1}	451	1	0.5	0
	1623–1873 K	6.45×10^3 atm$^{-1}\cdot$s$^{-1}\cdot$µm	88	1	0.5	1

When magnetite concentrate is reduced by a mixture of H_2 + CO, the CO enhances the rate of reaction between H_2 and iron oxide, most likely due to the effect of CO on the morphology of the reduced iron by forming whiskers which was observed in a separate study [22]. Taking this into consideration, Fan et al. [17] developed the following rate equations for the reduction of magnetite concentrate particles by H_2+CO mixtures in the two temperature ranges of 1423–1623 K (1150–1350 °C) and 1623–1873 K (1350–1600 °C):

$$\frac{dX}{dt} = \left(1 + 1.3\cdot\frac{p_{co}}{p_{co}+p_{H_2}}\right)\cdot\left.\frac{dX}{dt}\right|_{H_2} + \left.\frac{dX}{dt}\right|_{CO} \quad 1423\ \mathrm{K} < T < 1623\ \mathrm{K} \quad (2)$$

$$\frac{dX}{dt} = \left(1 + (-0.01T + 19.65)\cdot\frac{p_{co}}{p_{co}+p_{H_2}}\right)\cdot\left.\frac{dX}{dt}\right|_{H_2} + \left.\frac{dX}{dt}\right|_{CO} \quad 1623\ \mathrm{K} < T < 1873\ \mathrm{K} \quad (3)$$

where $\left.\frac{dX}{dt}\right|_{H_2}$ and $\left.\frac{dX}{dt}\right|_{CO}$ represent the rates of reduction individually by H_2 and CO, respectively, obtained from Equation (1) with the parameters listed in Table 1.

Similar rate measurements were also done with hematite concentrate [18,23,24]. It was conclusively confirmed by the work described above that iron ore concentrate particles can be >95% reduced by hydrogen in several seconds of residence time typically available in a flash reactor at 1473 K or above.

4. Tests in a Laboratory Flash Reactor

Based on the results of kinetic feasibility discussed above, reduction tests were conducted by Sohn et al. [8,25,26] in a laboratory flash reactor shown in Figure 2. An industrial flash reactor would be significantly different from a laminar-flow reactor (LFR) used for the rate measurement, including the fact that an oxy-fuel burner would be the main source of heat and the amount of excess reducing gases would be much lower (20–100%). The laboratory flash reactor had many of the features of an industrial flash reactor. Other experimental details can be found elsewhere [25–28].

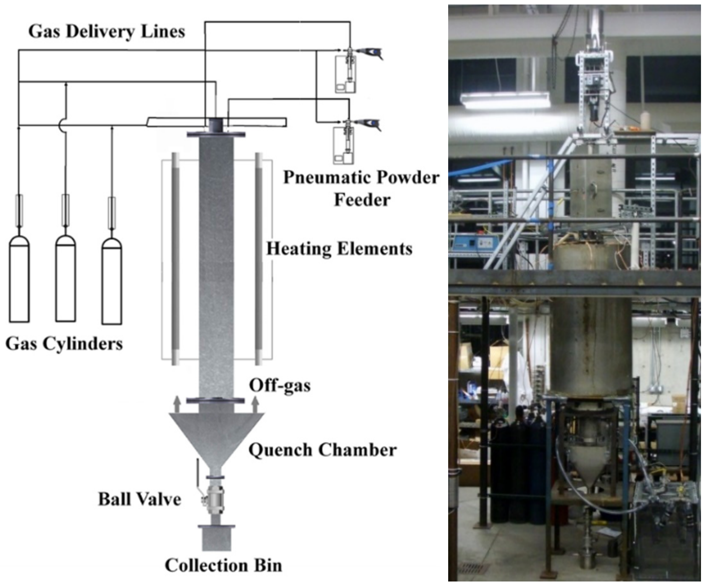

Figure 2. The Utah laboratory flash ironmaking reactor (I.D. 0.19 m and length 2.13 m).

Experiments were performed with either hydrogen or methane and with different modes of gas and particle feeding, the results of which were analyzed with the aid of computational fluid dynamics (CFD) simulations.

The tests and simulation using the laboratory flash furnace produced useful information, the most important of which can be summarized as follows:

- Iron can be obtained from iron concentrates by flash reduction using partial combustion of gaseous fuels: hydrogen, natural gas, or a mixture thereof.
- The configuration of fuel gas and oxygen feeding is important in terms of temperature uniformity and accompanying concentrate feeding mode. A flame generated by central feeding of the gaseous fuel surrounded by oxygen flow promoted temperature uniformity and allowed solid feeding through the center of the flame.
- The best position for concentrate feeding is near but outside the flame. This configuration works with either mode of gas feeding, fuel gas surrounded by oxygen, or vice versa.

5. Operation of Pilot Plant with Flash Reactor

A pilot flash reactor (PFR) capable of operating at 1200–1600 °C with a concentrate feeding rate of 1–7 kg/h, shown in Figure 3, was operated at the University of Utah [27]. This reactor was the first flash ironmaking reactor where the heat and reductant are produced by partial oxidation of natural gas or hydrogen with tonnage oxygen.

Figure 3. The pilot plant with a flash reactor installed at the University of Utah.

The PFR consisted of a reactor vessel, a vessel roof, burners, a quench tank, off-gas piping, a flare stack, an off-gas analyzer, a gas valve train, a water-cooling system, gas leak detectors, a concentrate feeding system, and human-machine interface. Figure 4 shows the main components of the reactor body. Only the very salient features will be described here, and other details of the facility and its operation are described elsewhere [27].

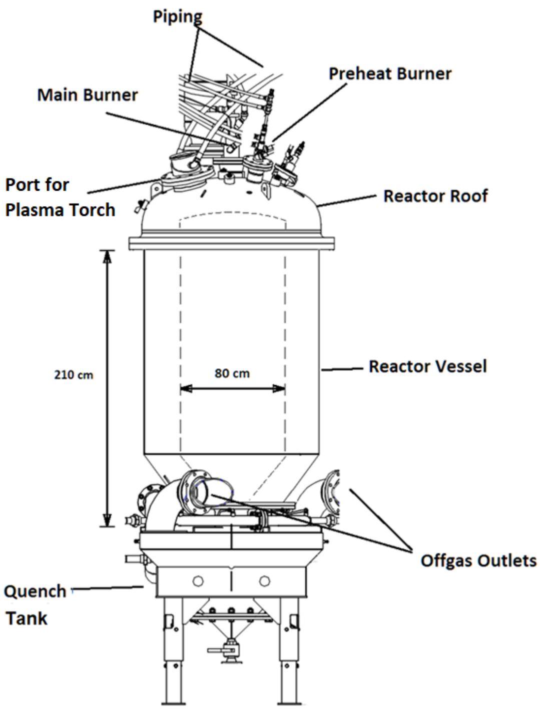

Figure 4. Schematic diagram of the pilot flash reactor (PFR).

5.1. Burners

The PFR had 3 burners: a preheat burner, the main burner, and a plasma burner. Figure 5 shows a schematic diagram for the cross section of the preheat burner and the main burner.

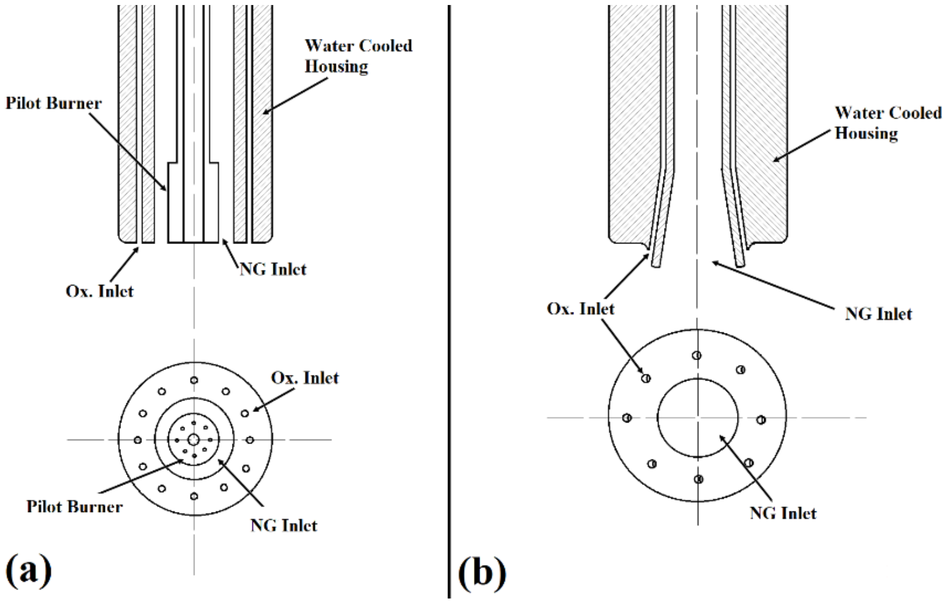

Figure 5. Schematic diagrams for (**a**) preheat burner and (**b**) main burner. NG stands for natural gas and Ox for oxygen.

5.2. Concentrate Feeding System

The concentrate was fed into the reactor using an HA5171P-D powder feeder supplied by HAI, Placentia, CA, USA. This pneumatic powder feeder was used to feed magnetite concentrate to the reactor at a feeding rate of 1–7 kg/h. Nitrogen gas at a flow rate of 11 standard liters per minute (SLPM) was used as the carrier gas. The particles were fed through feeding inlets on the sides of the main burner. This was determined based on the results obtained from the laboratory flash reactor.

5.3. Human Machine Interface

The human machine interface (HMI) consists of the main programmable logic controller (PLC) and a computer. The main PLC was connected to all the different parts of the system and to the computer where the operator could monitor all the different parts and run the reactor. The programming in the main PLC was responsible for all the safety and emergency steps. The main PLC was supplied by ACS company, Boise, ID, U.S. Figure 6 shows a screen shot where all the parameters of the reactor were displayed and controlled.

5.4. Operation of the PFR

All the components of the reactor were installed and a leak test was performed on the vessel by capping the off-gas pipes and pressurizing the system to 2.0 atm for 45 min to make sure that there were no leaks from any components. The system was preheated to the target temperature with a heating rate of 90–95 °C/h which was the maximum heating rate that could be used to avoid any damage to the refractories. The heating cycle was automatically controlled by the HMI and the flow rates of natural gas and oxygen were varied based on the measured temperature from the reactor vessel.

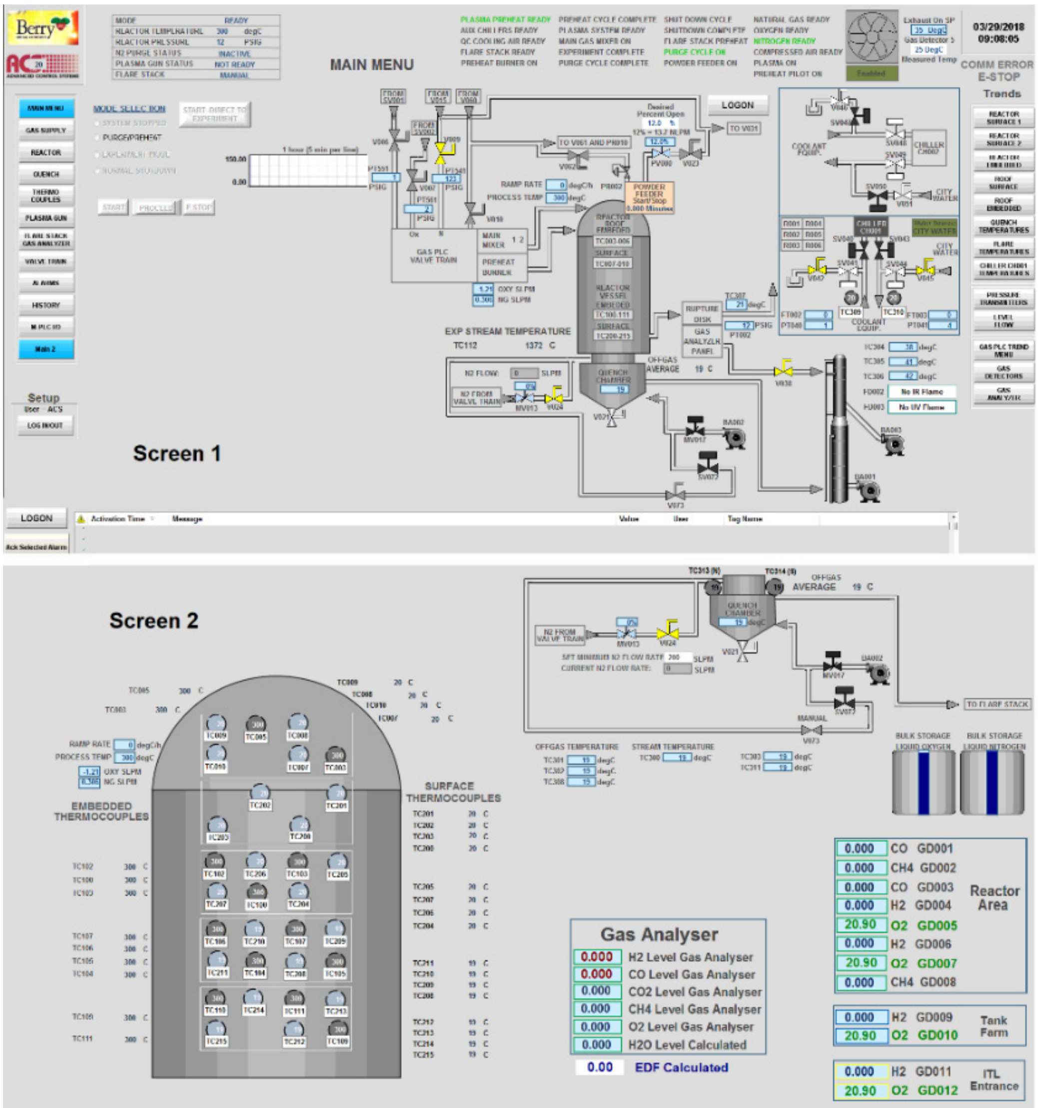

Figure 6. The controlling screen for the human machine interface (HMI).

5.5. Results from PFR Runs

This reactor was simulated by CFD to optimize the operating conditions to achieve high reduction degree at the optimum conditions and reactor sizes to be used in an industrial reactor [29]. The results obtained from the developed CFD model were compared to the actual results of the reactor operation and good agreement was achieved. Table 2 shows the results of the runs performed in the reactor.

Different experimental runs were designed in this reactor to yield a wide range of reduction degrees at less than complete reduction to better examine the effects of the operating conditions and validate the CFD model in these different conditions. The results showed good reproducibility within ±5% of the average reduction degree. This represents a very high degree of reproducibility, considering the complexity of the operation and design of this large unit.

Table 2. The results of runs performed in the pilot flash reactor (PFR).

Inner Wall Temperature (°C)	Magnetite Concentrate Feeding Rate (kg/h)	Gas Flow Rate * Main Burner NG (SLPM) **	O$_2$ (SLPM)	H$_2$ EDF †	Nominal Residence Time (s)	RD †† (%)
1200–1130	5.0	404	321	0.76	12.5	65
1290–1220	1.8	410	293	0.84	12.0	79
1290–1210	2.9	410	293	0.96	12.0	82
1290–1230	2.5	358	270	1.00	13.3	83
1290–1240	3.5	512	327	1.07	10.2	76
1330–1230	4.7	330	200	1.36	15.3	89
1330–1230	4.5	330	200	1.44	15.3	87
1330–1230	5.2	500	290	3.00	10.6	80
1330–1230	4.3	500	290	3.00	10.6	82
1355–1260	5.5	235	190	0.03	18.3	7
1350–1300	4.0	255	209	0.15	17.0	49
1350–1270	4.5	275	212	0.20	16.2	31
1340–1280	5.0	280	209	0.21	16.2	37
1350–1290	4.6	280	230	0.50	15.6	80
1400–1300	6.3	300	240	0.82	14.4	88
1400–1300	5.0	330	200	1.51	14.6	100
1415–1350	4.5	220	191	0.07	18.0	18
1410–1360	4.0	240	195	0.33	17.1	32
1410–1330	5.0	295	221	0.50	14.7	66
1410–1330	6.0	300	210	0.70	14.9	74
1410–1320	5.0	300	210	0.82	14.9	82

* The flow rates of NG and O$_2$ in the pilot burner were 9.6 and 37.6 SLPM, respectively. The flow rate of N$_2$ in the powder feeder was 10.7 SLPM. ** SLPM stands for standard liters per minute. † EDF stands for excess driving force of reactant gas over the equilibrium value. †† RD stands for reduction degree.

6. Design of Medium-Size Flash Ironmaking Reactors

A reactor with a capacity of 100,000 t/y of iron was designed to further test the feasibility of FIT in this range of production rate. For the proper design and scale-up of such reactors, it is essential to have information on the temperature and species distribution, gas and particle flow patterns. This information is difficult or even impossible to obtain from experiments. With computational fluid dynamics (CFD) modeling, it is possible to gain such insights into these critical parameters that are essential in reactor design.

Here, two types of reactors were designed. The first type was to produce metallic iron in solid state. The typical operating temperature in this case is around 1300 °C. The solid-state product collected could be charged into an electric arc furnace in the steelmaking process. The second type is to produce iron in the molten state, which is typically operated at a temperature of around 1600 °C, and can lead to direct steelmaking combined with flash reduction or charged into a basic oxygen furnace or an electric arc furnace without further treatment.

6.1. Geometries and Dimensions

Sketches of possible configurations of flash ironmaking reactors are shown in Figure 7. Depending on the operating conditions, the main body of the reactor is either made up of a cylindrical part and a conical part or a cylindrical shaft only. Under solid state operating conditions, a conical part near the exit of the reactor is needed for solid particle collection. If iron is produced in the molten state, a bath settler is needed below the shaft, as shown in Figure 1. Our focus is mainly on the shaft part of the reactor in this work as the reduction of concentrate particles mostly happens during their travel in the shaft.

With the same reactor volume, the design with a large height to diameter ratio leads to a long and thin reactor, while a small height to diameter ratio leads to a short and fat one as shown in Figure 7. In this study, two typical diameters, 4 m and 6 m, were tested. The diameter of the long and thin reactor was set to be 4 m. A diameter of 6 m was used for the short and fat reactor. The number of burners to be used is also an important factor in reactor design. Reactors with one burner and four burners were tested in this work. Before deciding on the number of burners to be used, the optimal value for the diameter was first determined under the one-burner design. The dimensions of the reactors simulated are listed in Table 3. The powders were fed through four feeding ports installed on the roof of the reactor. The four powder feeding ports were distributed evenly (90 degrees apart), as shown in Figure 8. The distance between each feeding port and the centerline of the reactor was equal to half of the radius.

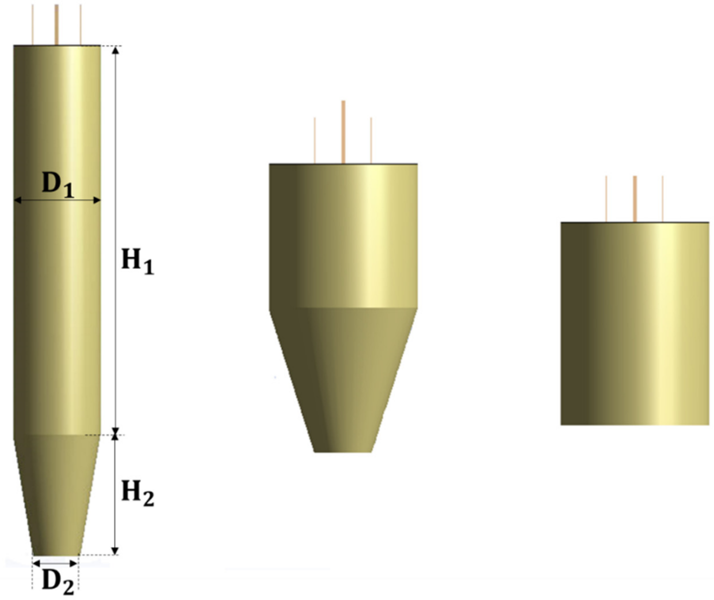

Figure 7. Sketches of possible configurations of flash ironmaking reactors.

Table 3. Dimension of reactors with one-burner.

D_1 (m)	D_2 (m)	H_1 (m)	H_2 (m)	Preheat Temp. (°C)	Designed Product Temp. (°C)	Design No.
4.0	2.0	12.0	6.0	600	1300	1
4.0	2.0	10.0	6.0	1000	1300	2
6.0	2.0	6.0	6.3	600	1300	3
6.0	2.0	6.0	5.0	1000	1300	4
4.0	–	13.0	–	1000	1600	5
6.0	–	9.0	–	1000	1600	6

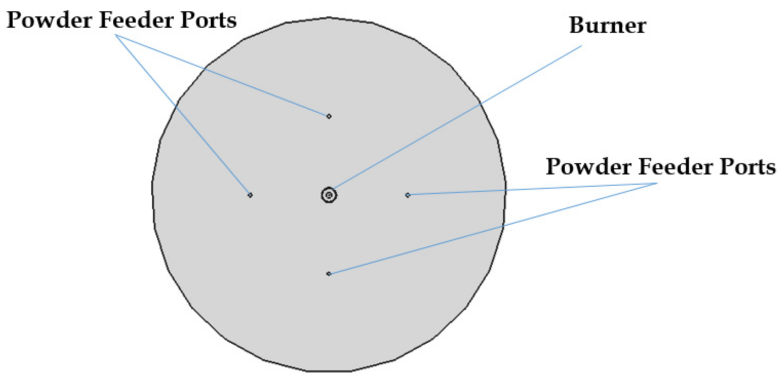

Figure 8. Distribution of the powder feeding ports on the roof of the reactor.

A nonpremixed burner with two oxygen slots and one natural gas slot, shown in Figure 9, was used in the simulation. The reactor wall consisted of three layers, namely, a refractory layer, an insulation layer, and a steel shell layer, as shown in Figure 10. The thicknesses of the refractory, insulation, and steel shell layers are kept at 0.15 m, 0.08 m, and 0.0254 m, respectively. Wall materials at those thicknesses were proved to be efficient in a pilot flash ironmaking reactor constructed on the campus of the University of Utah that was designed to operate from 1200 to 1600 °C. The properties of the wall materials are listed in Table 4.

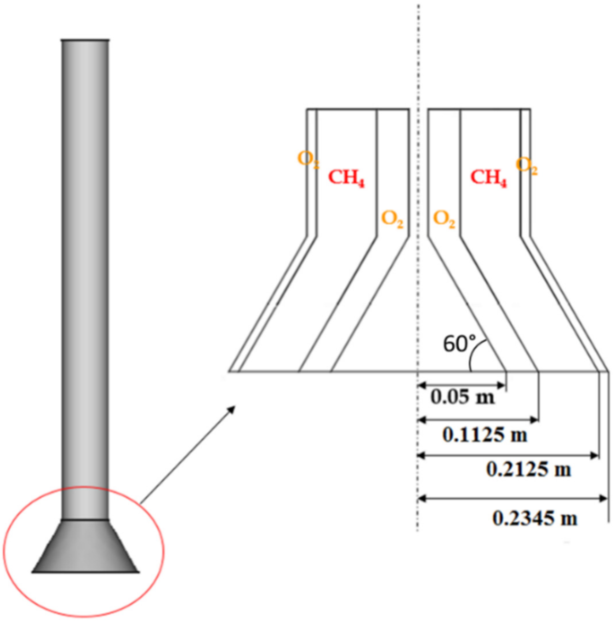

Figure 9. Burner configuration.

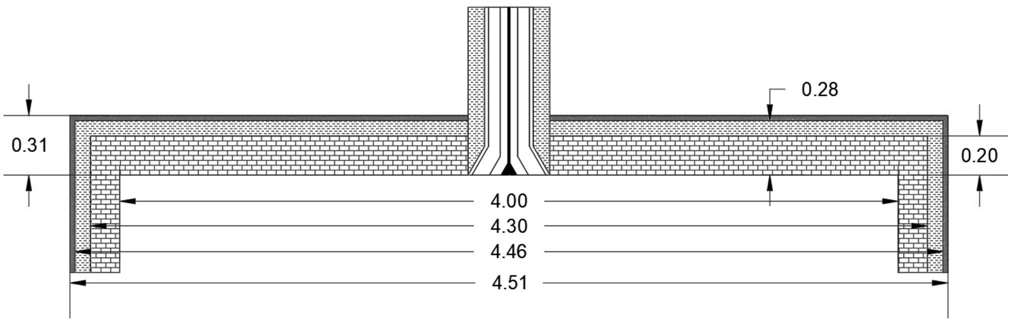

Figure 10. Reactor wall structure (unit in m).

Table 4. Wall material properties.

Wall Material	Thermal Conductivity ($W{\cdot}m^{-1}{\cdot}K^{-1}$)	Density ($kg{\cdot}m^{-3}$)	Specific Heat ($J{\cdot}kg^{-1}{\cdot}K^{-1}$)
Refractory	$10^{-6}\,T^2 - 0.0032\,T + 4.5396$	2890	$0.2965\,T + 362$
Insulation	$3 \times 10^{-8}\,T^2 + 4 \times 10^{-5}\,T + 0.1797$	1081	714
Steel shell	50	7850	470

6.2. Operating Conditions

The fuel entering the reactor consisted of fresh natural gas and recycled H_2, which were partially oxidized by oxygen to generate the heat needed for the reaction as well as the reducing gases CO and H_2. The recycled H_2 is recovered from the off-gas which always contains a significant amount of hydrogen because the reduction of FeO by hydrogen is limited by equilibrium. The actual composition of natural gas was 96% CH_4, 2% C_2H_6, and 2% nitrogen by volume. It makes the CFD simulation program, including the combustion calculation, rather complicated to add the oxidation of C_2H_6, even if its amount is small.

Considering that the amount is small and also that its oxidation produces the same gases as CH_4, the amount of C_2H_6 was converted to the equivalent amount of CH_4. In terms of heat production, 1 mol% of C_2H_6 is equivalent to 2.6 mol% of CH_4 and in terms of hydrogen and carbon monoxide production, 1 mol% of C_2H_6 is equivalent to 2 mol% of CH_4. Thus, to correct for the presence of the small amount of C_2H_6, 1 mol% of C_2H_6 was treated as being equivalent to 2.3 mol% of CH_4. As a result, natural gas was considered as 98.1% CH_4 and 1.9% N_2. The input gases were preheated to a specified temperature before charging into the reactor to reduce the amount of input gases needed. In this work, two preheat temperatures (600 and 1000 °C) were investigated. The operating conditions are summarized in Tables 5–7.

Table 5. Operating conditions for solid product with input gases preheated to 600 °C.

Feed	Flow Rate (kg/s)	Preheat Temp. (°C)
Natural Gas	1.15	600
Recycled H_2	0.43	600
Oxygen	2.19	600
N_2 (Carrier Gas)	0.07	25
Concentrate	5.20	25

Table 6. Operating conditions for solid product with input gases preheated to 1000 °C.

Feed	Flow Rate (kg/s)	Preheat Temp. (°C)
Natural Gas	0.91	1000
Recycled H_2	0.36	1000
Oxygen	1.54	1000
N_2 (Carrier Gas)	0.07	25
Concentrate	5.20	25

Table 7. Operating conditions for molten product with input gases preheated to 1000 °C.

Feed	Flow Rate (kg/s)	Preheat Temp. (°C)
Natural Gas	0.91	1000
Recycled H_2	0.36	1000
Oxygen	1.54	1000
N_2 (Carrier Gas)	0.07	25
Concentrate	5.20	25

The concentrate feeding rate was calculated based on 340 normal operating days in a year, 70 wt.% total iron content in the concentrate and product metallization of 95%. As is seen from Tables 5 and 6, when the preheat temperature was lower, the flow rates of fuel and oxygen had to be increased to maintain the temperature in the reactor at 1300 °C.

Steady state conditions were simulated in this work. The Euler–Lagrange approach was used to model the two-phase flow, in which the gas phase was treated as a continuum in the Eulerian frame of reference while the solid phase was tracked in the Lagrangian mode. A two-way coupling approach between the gas and solid phases was used in the simulation. The CH_4-O_2 combustion mechanism available in the literature [30] was used. In a large reactor, an efficient cooling method, such as copper stove cooling technology, is usually necessary to cool the outer surface of the reactor to an acceptable temperature. The incorporation of such cooling system significantly complicated the model. For simplicity, the outer surface of reactor in this work was set to be 60 °C for all the calculations.

6.3. Results and Discussion

The mass-weighted average metallization degrees at the exit of reactor in all the designs listed in Table 3 were aimed to be 95%.

6.3.1. One-Burner Design

Typical velocity vector fields in the plane that passes through the center of two powder feeding ports are shown in Figure 11. It is seen from these figures that due to the high-velocity jets erupting from the burner nozzles, recirculation zones formed in regions close to the reactor inner wall in the top part of the reactor. In design No.1, the particles entering the reactor may be pushed to the reactor wall by the hot, high-velocity gas coming out of the flame region as seen in Figure 11a. The particles being pushed towards the wall may cause the sticking problem. In design No.3, the concentrate particles were less affected due to its larger diameter. Design No.3 gave a better flow field in this case.

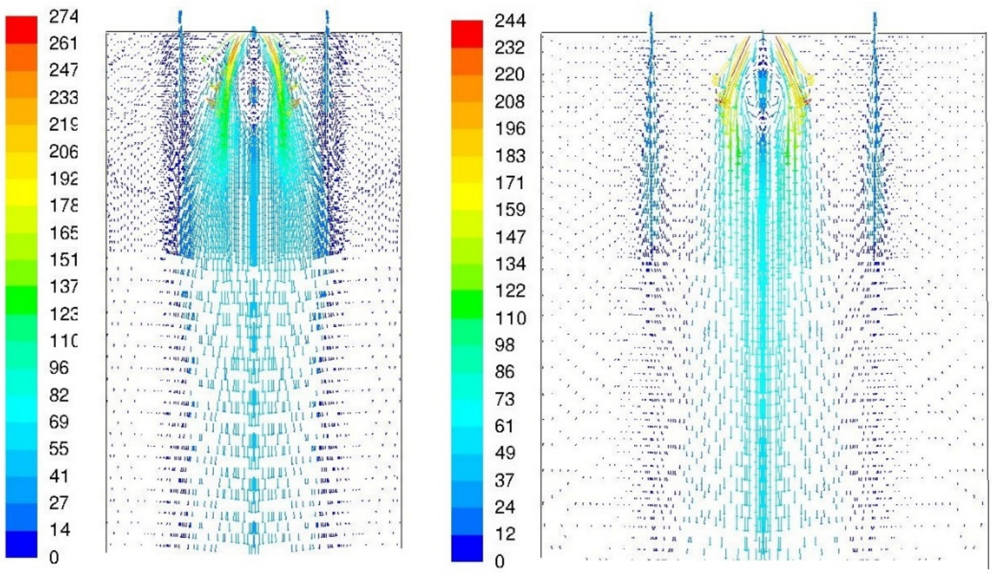

(**a**) (**b**)

Figure 11. Velocity vector field in the plane passing through the centers of two powder feeding ports: (**a**) design No. 1 and (**b**) design No. 3 under operating conditions listed in Table 5 (unit in m/s).

Typical particle distributions are shown in Figure 12. It is evident that when the reactor diameter was 4 m, the particle concentration near the wall was higher than that when the reactor diameter was increased to 6 m. The particles were more evenly distributed in the top part in the latter case.

The temperature distributions in the same plane above are shown in Figure 13. It is seen that in the reactor with a diameter of 4 m, the particles were close to the flame region in the top part of the reactor, especially in design No. 1, which may cause the particles to melt. For the reactor with a diameter of 6 m, the particle-laden streams were farther away from the flame region.

Heat loss is another criterion to look at in the reactor design. The heat loss through the walls in each design was calculated and listed in Table 8. In order to help better evaluate the energy efficiency of each reactor, the percentage of energy loss (the percentage of heat loss from the heat generated from combustion plus the amount of sensible energy of the input gases) is also calculated. The numbers indicated that reactors with a diameter of 6 m had a smaller value of heat loss than reactors with a diameter of 4 m, as expected, but this result gives a numerical indication of how the heat loss compares between the two cases.

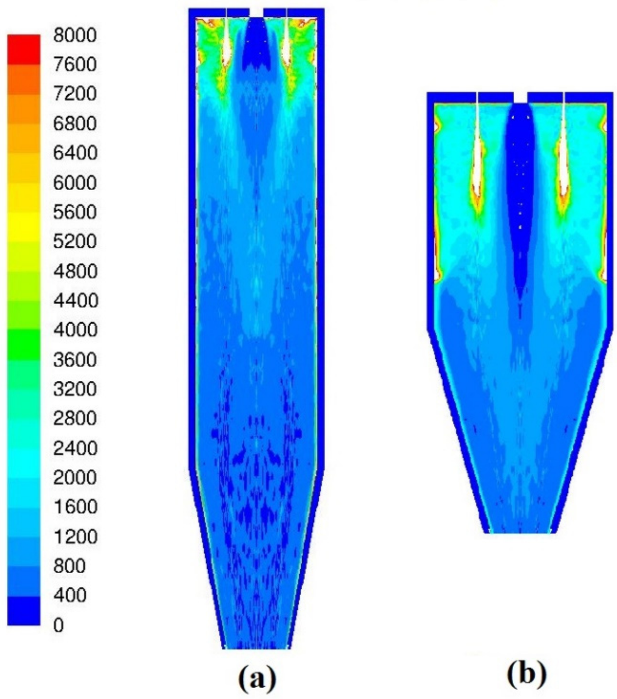

Figure 12. Particle number density (particles/cm^3) in the plane passing through the centers of two powder feeding ports: (**a**) design No. 1 and (**b**) design No. 3 under operating conditions listed in Table 5.

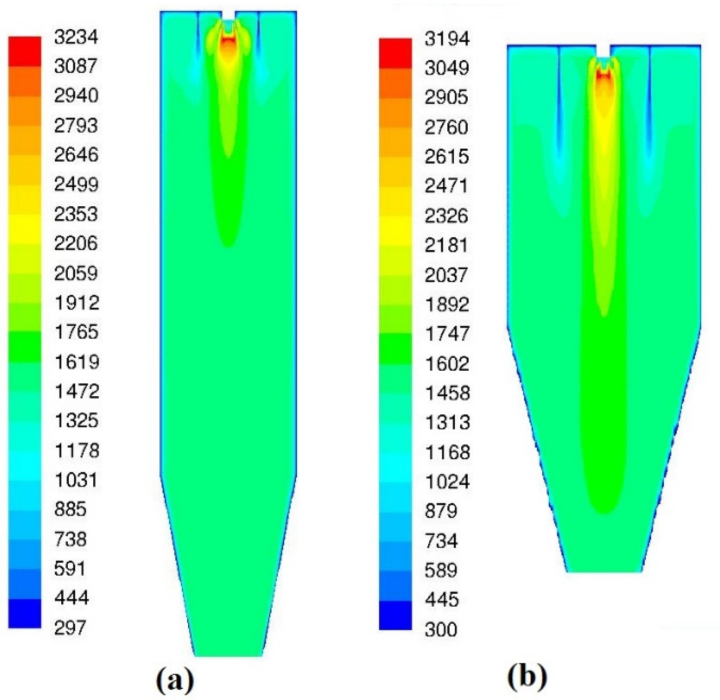

Figure 13. Temperature (in K) distribution in the plane passing through the centers of two powder feeding ports: (**a**) design No. 1 and (**b**) design No. 3 under operating conditions listed in Table 5.

Table 8. Heat loss and heat generated from partial combustion.

Design No.	Heat Loss (MW)	Heat Generated (MW)	Sensible Heat of Input Gases from Preheating (MW)	Percentage (%)
1	0.72	19.26	6.82	2.76
2	0.55	12.31	9.92	2.47
3	0.62	19.26	6.82	2.38
4	0.45	12.31	9.92	2.02
5	0.68	20.58	13.6	1.99
6	0.61	20.58	13.6	1.79

Therefore, the geometry used in design No. 6 will be used as the design of the flash reactor that is operated to produce molten iron. The design of a flash reactor that operates to produce a solid product will be further discussed in the next section. The species distributions in designs No. 5 and No. 6 are shown in Figures 14 and 15. The main component gases outside the flame region reached equilibrium quickly and were uniformly distributed. The mole fractions of H_2, H_2O, and CO at the exit of two reactors (outside the flame region) were the same at 0.48, 0.32, and 0.13, respectively.

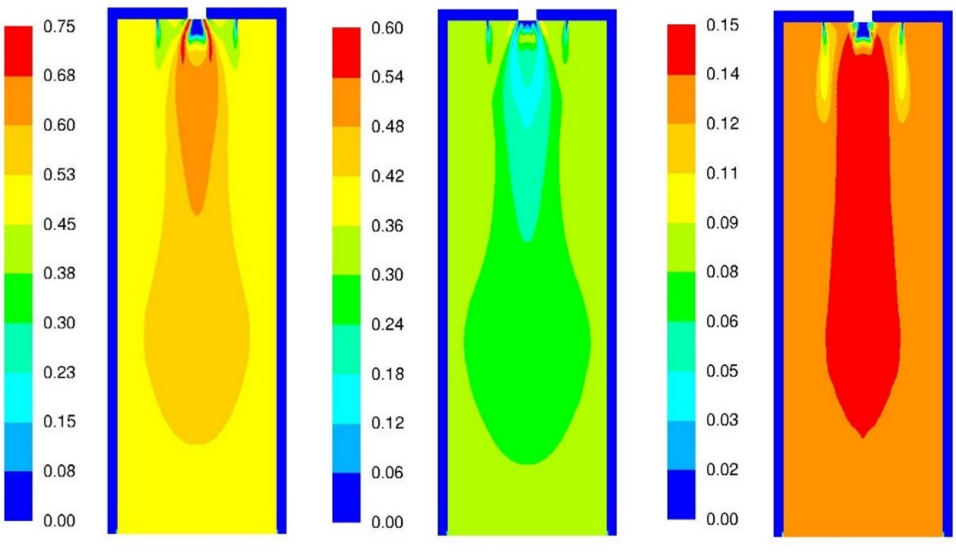

Figure 14. Species distribution in the plane passing through the centers of two powder feeding ports of design No. 5: (**a**) H_2, (**b**) H_2O, and (**c**) CO.

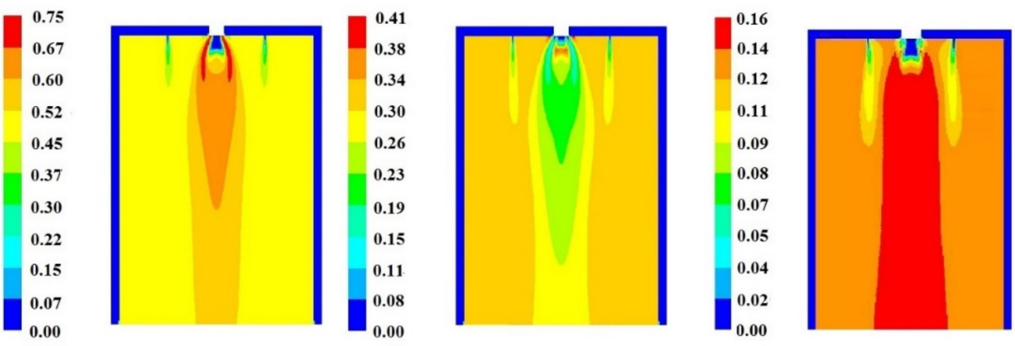

Figure 15. Species distribution in the plane passing through the centers of two powder feeding ports of design No. 6: (**a**) H_2, (**b**) H_2O, and (**c**) CO.

6.3.2. Four-Burner Design

The flash ironmaking reactor with the one-burner had uneven distribution of gaseous species and temperature as well as high particle concentrations near the wall in the top part of the reactor, as seen, respectively, from Figures 12 and 13 due to the strong recirculation flow. In this section, the four-burner design is discussed. The distribution of the four burners on the roof of the reactor is shown in Figure 16.

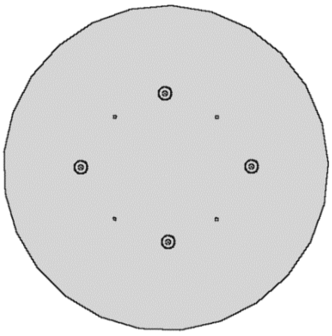

Figure 16. Distribution of the burners on the roof of the reactor. The large openings are burners and the small openings are powder feeding ports.

The four burners were evenly distributed 90 degrees apart on the roof. The distance between the burner and the centerline of the reactor was equal to half of the radius. The powder feeding ports were symmetrically placed in-between two burners. The distance between the powder feeding port and the centerline of the reactor was also equal to half of the radius. The burners used in this case were different from the one used in the one-burner design. The radial velocity was eliminated by replacing the conical burner tip with a straight concentric design, as shown in Figure 17. The natural gas stream was in the middle and was surrounded by two oxygen streams.

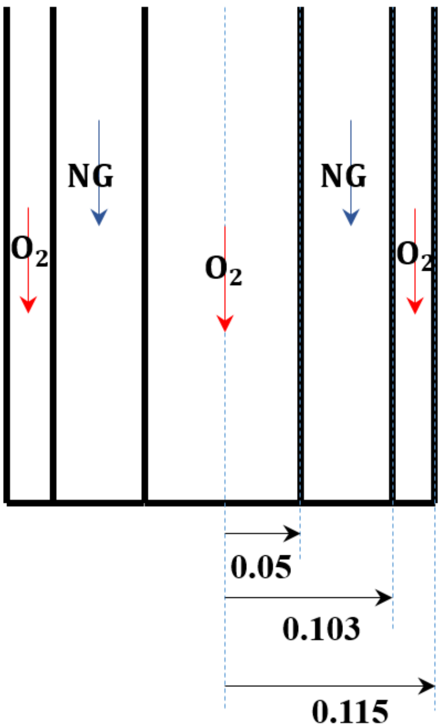

Figure 17. Burner configuration and dimension (unit in m).

The same dimension as design No. 3 in Table 3 was used in this simulation. The reactor diameter was chosen as 6 m. The same three layers of walls were also used in this design. The operating conditions listed in Table 5 were used as the reactor was designed to produce solid iron particles.

The velocity field in the plane that crosses the center of two powder feeding ports is shown in Figure 18. The radial velocity component near the burner was smaller than that in the one-burner design. The particle number density distribution is shown in Figure 19. The number density of the concentrate particles close to the wall was greatly reduced, making particle sticking to the wall much less likely.

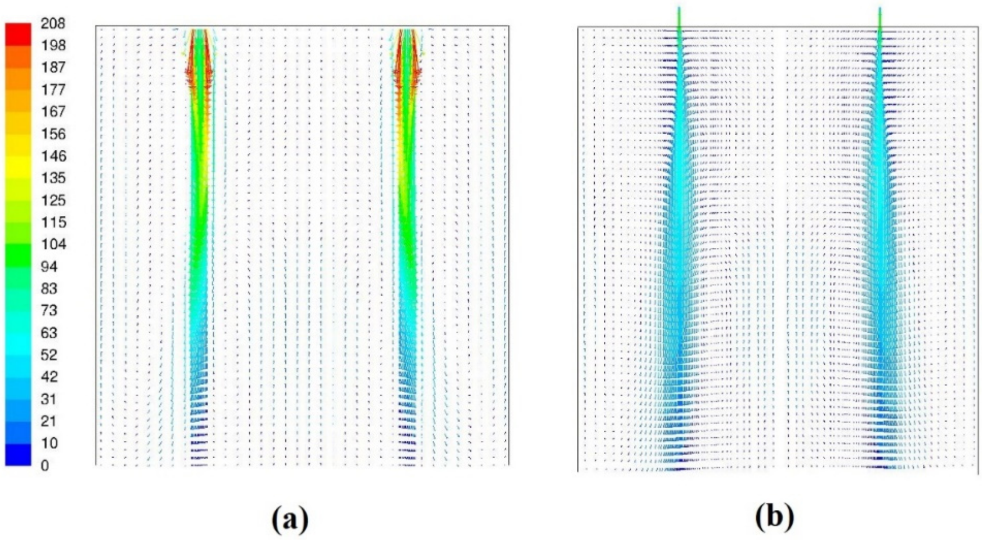

Figure 18. Velocity field in the plane passing through (**a**) the centers of two opposite burners and (**b**) the centers of two opposite powder feeder ports (unit in m/s).

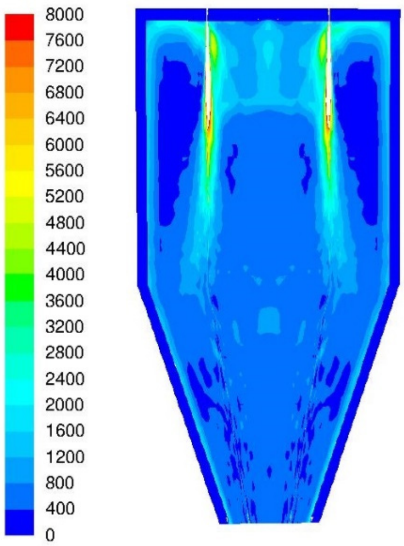

Figure 19. Particle number density (particles/cm^3) in the plane passing through the centers of two opposite powder feeding ports.

The temperature distributions are shown in Figure 20. Compared with the one-burner design, the particle stream regions in the four-burner design were less exposed to the high temperature of the flame. The consequence of this is that melting of the concentrate particles was less likely to happen so that the reduction of the concentration particles was not affected. Better temperature homogeneity was also seen in this reactor as four burners were used. As a result, the energy generated from the partial combustion was more uniformly distributed inside the reactor. The averaged product temperature at the exit of the reactor was 1278 °C rendering the mass averaged reduction degree of the product as 93%. The heat loss of this reactor was 0.65 MW, which is somewhat greater than the heat loss in design No. 3. This is expected as the high temperature region in Figure 20 is closer to the wall than that in Figure 13.

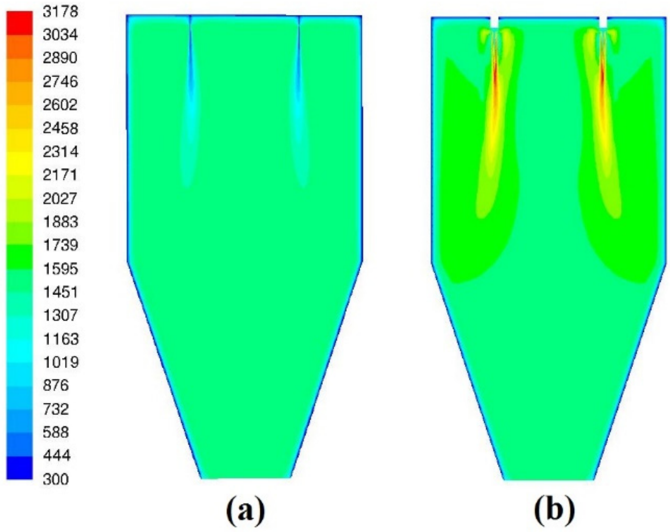

Figure 20. Velocity vector field in the plane passing through (**a**) the centers of two opposite burners and (**b**) the centers of two opposite powder feeder ports (unit in m/s).

The main species distribution inside the reactor is shown in Figures 21 and 22. No noticeable change in the CO and CO_2 mole fractions outside the flame region was seen as the reduction of magnetite concentrate particles was done by H_2. The mole fractions at the exit of the reactor for H_2, H_2O, CO, and CO_2 were 0.47, 0.31, 0.13, and 0.025, respectively.

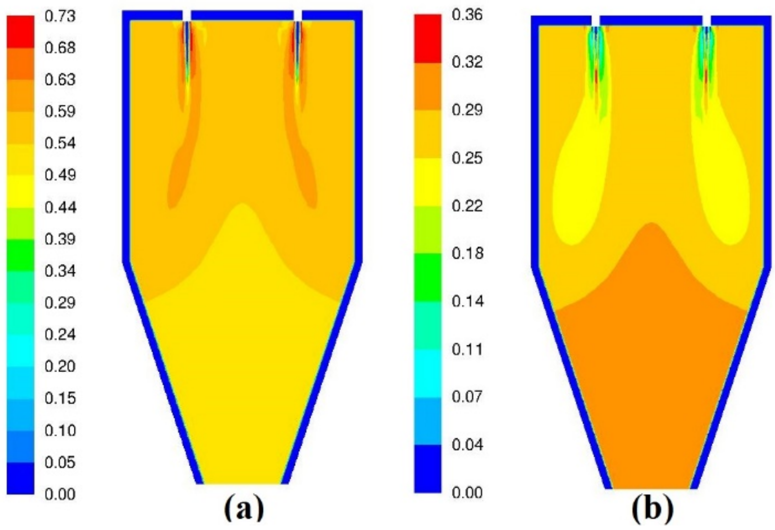

Figure 21. Species distribution in the plane passing through the centers of two opposite burners: (**a**) H_2 and (**b**) H_2O.

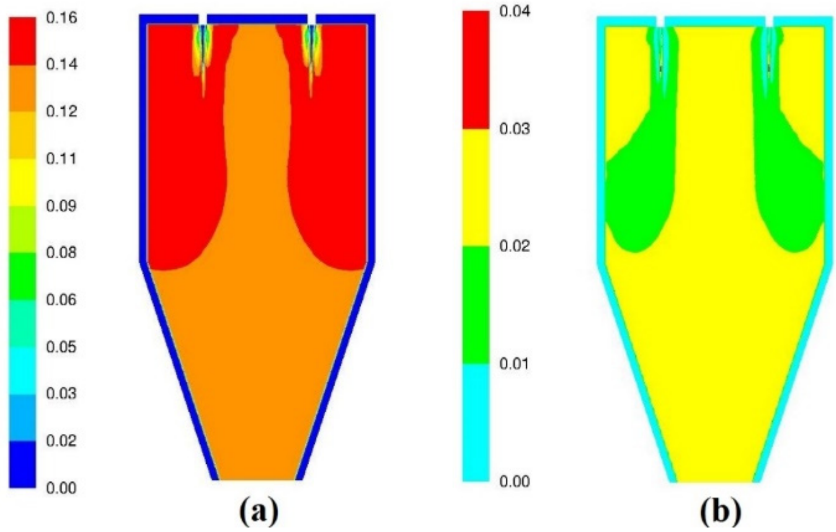

Figure 22. Species distribution in the plane passing through the centers of two opposite burners: (**a**) CO and (**b**) CO_2.

6.3.3. Summary

Flash ironmaking reactors of different geometrical dimensions with a capacity of producing 100,000 t/y of metallic iron were designed. The metallization degrees of product from these reactors were sufficiently high for use in the subsequent steelmaking step. In the one-burner design, reactors with a diameter of 6 m gave better particle and temperature distributions than reactors with a diameter of 4 m. Better energy efficiency in terms of heat loss was also seen for reactors with a diameter of 6 m. A high particle number density near the wall was less likely in design No. 6. A reactor with a diameter of 6 m and 4 burners was also simulated. The larger burner number led to a better particle distribution. The particle distribution in this reactor showed a lower probability of particle sticking compared with design No. 3 with a single burner design. All these results may be expected qualitatively, but the CFD simulations present the possibility of yielding quantitative effects of design variation.

7. Design of Industrial Flash Ironmaking Reactors

An industrial ironmaking plant should have a capacity to produce at least 0.3–1.0 million t/y of iron to be competitive with modern blast furnaces, which typically produce 0.3–3.0 million t/y of iron. The same model that was previously described was used for designing two industrial reactors capable of production in this range. A multi-burner configuration was shown in the previous section to have a number of advantages, but for the larger reactors the computational time and difficulties were rather prohibitive for this work. Thus, the industrial reactors were designed to have a single burner in the center of the reactor with four feeding ports. Further, the simulated reactor was designed to produce solid iron particles as opposed to molten iron, as the near-term application of the novel flash ironmaking technology is to produce direct reduced iron (DRI) rather than to operate for direct steelmaking as shown in Figure 1. It is hoped that what we learn from this work will provide helpful information and insight in designing future industrial flash ironmaking reactors.

7.1. Dimensions and Operating Conditions

Table 9 shows the operating conditions of the two industrial reactors. The smaller reactor produces 0.3 million tons of iron per year while the larger reactor produces 1.0 million tons of iron per year.

Table 9. Operating conditions of the two industrial reactors.

Parameter	Reactor 1	Reactor 2
Target production of iron in million t/y.	0.3	1.0
Feed of the magnetite concentrate in million t/y.	0.415	1.38
Natural gas feeding rate in m^3/s	17.5	45.8
Oxygen feeding rate in m^3/s	13.2	34.7
Expected excess of hydrogen at full reduction (EDF)	0.3	0.3

Schematic representations of the reactor and the burner are shown in Figures 23 and 24, respectively, while the dimensions for the two reactors are shown in Table 10.

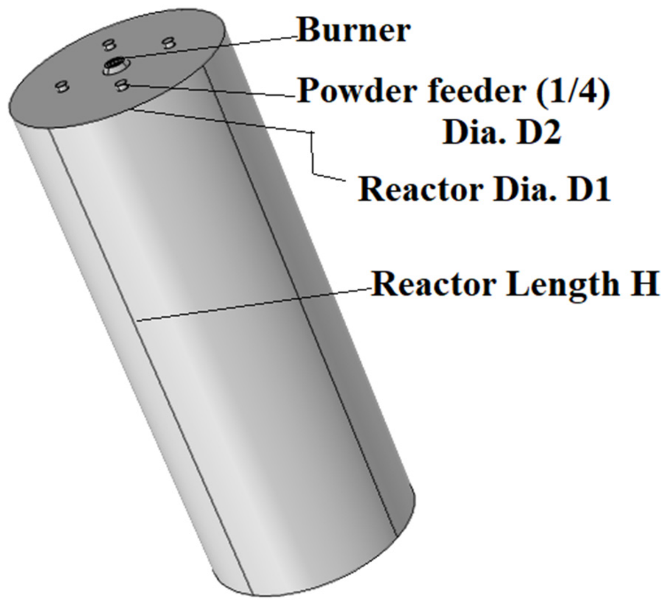

Figure 23. Schematic representation of the industrial reactor.

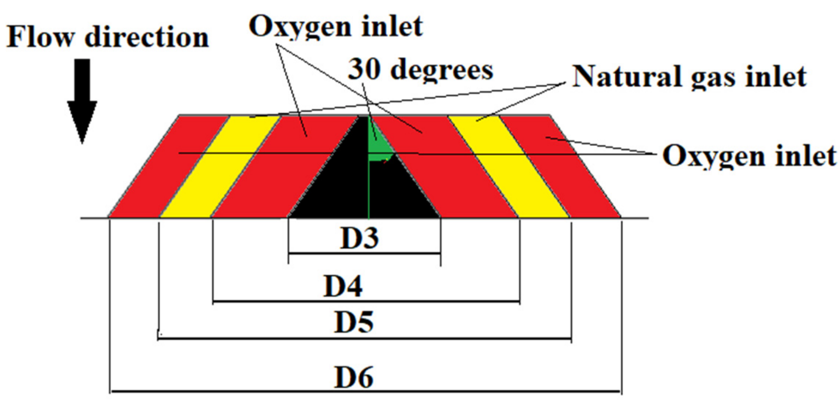

Figure 24. Schematic representation of the burner.

It is noted that the radial location of the powder feeders was half the radius of the reactor. Furthermore, the volumetric flow rates of oxygen in inlets 1 and 2 were equal.

Table 10. The dimensions of the industrial reactors.

Parameter	Definition	Reactor 1 (m)	Reactor 2 (m)
H	Height	35.0	35.0
D1	Inner diameter	7.0	12.0
D2	Diameter of powder feeder (4 feeders)	0.05	0.30
D3	Inner diameter of the oxygen inlet 1	0.02	0.02
D4	Outer diameter of the oxygen inlet 1	0.26	0.8
D5	Outer diameter of the natural gas inlet	0.44	1.6
D6	Outer diameter of the oxygen inlet 2	0.51	1.8

7.2. Meshing

The industrial reactors were designed to have a single burner in the center of the reactor with four feeding ports evenly distributed and have the same radial position equal to half the radius of the reactor. The symmetry of the reactor was used to decrease the computational time by taking a quarter of the reactor as a representation for the entire reactor.

The mesh consisted of 264,000 hexahedral cells in the smaller reactor and 279,000 hexahedral cells in the larger reactor. The top section of the meshing for Reactor 2 is shown in Figure 25.

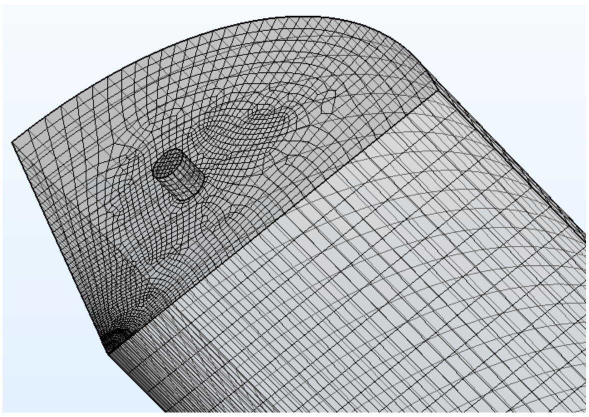

Figure 25. Meshing of the top section for a quarter of Reactor 2.

7.3. Results and Discussion

Mass weighted average gas composition and product metallization at the outlet: A velocity of 100 m/s was used for the inlet gases in Reactor 1, while for the larger Reactor 2 the area of the burner was increased and thus the inlet velocity was 37 m/s. The products from reactor exit can tell us the efficiency of the design. As shown in Table 11, the metallization degrees of the products from the two reactors were nearly identical at >90%. The higher temperature of the gas mixture in Reactor 2 indicates that heat loss was lower from it, as expected.

Table 11. Average gas composition and metallization degree at reactor exit.

Reactor	T (K)	H_2	CO	CO_2	H_2O	Metallization (%)
1	1519	40.2	26.3	5.9	24.1	91.2
2	1578	39.9	26.6	5.7	24.8	91.4

Contours of gas velocity, temperature, and product gas contents: The contours of different variables in the reactor help to evaluate the performance of the reactor. Figure 26 shows the contours of velocity magnitude in the gas phase, Figure 27 shows the temperature distribution, and the H_2, CO, H_2O, and CO_2 gases content are shown in Figures 28–31, respectively.

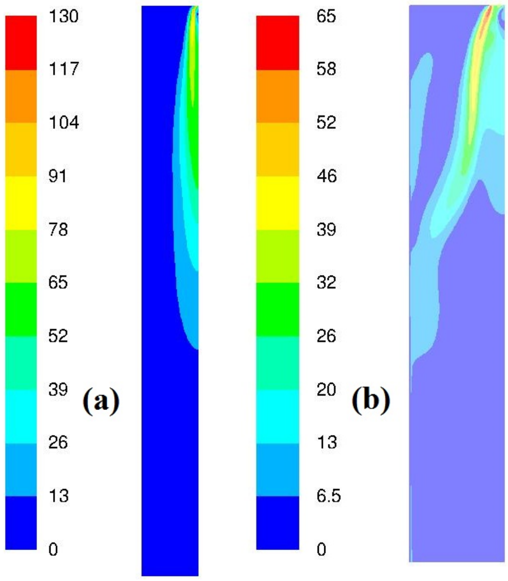

Figure 26. Gas velocity magnitude in m/s where the right vertical line represents the axis of symmetry: (**a**) Reactor 1 and (**b**) Reactor 2.

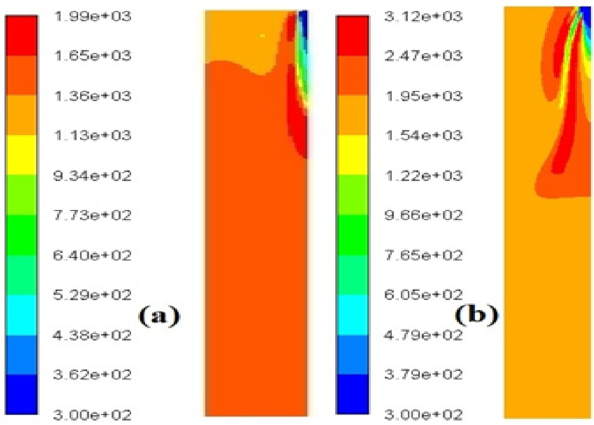

Figure 27. Contours of gas temperature (in K) where the right vertical line represents the axis of symmetry: (**a**) Reactor 1 and (**b**) Reactor 2.

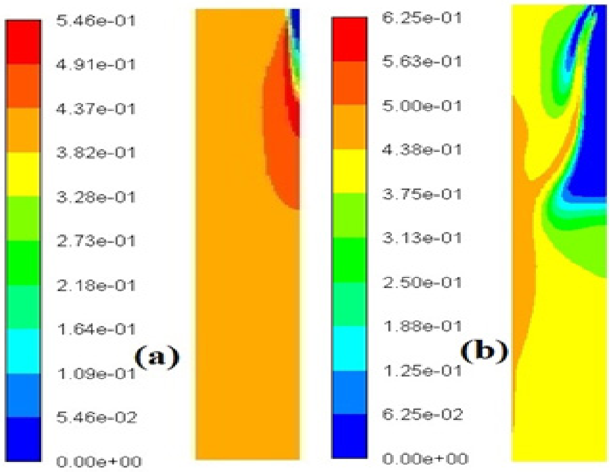

Figure 28. Contours of H_2 content in mole fraction where the right vertical line represents the axis of symmetry: (**a**) Reactor 1 and (**b**) Reactor 2.

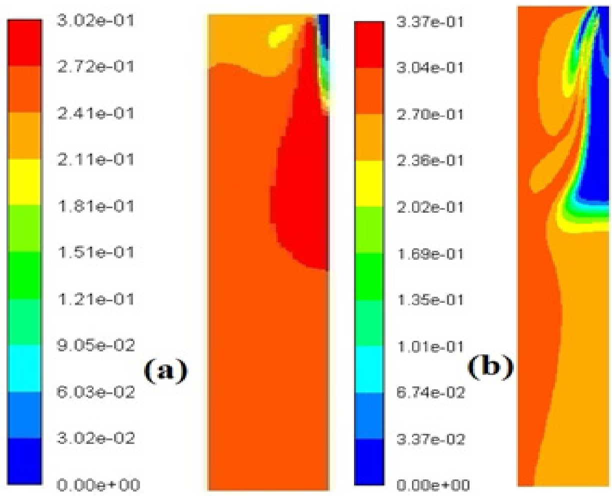

Figure 29. Contours of CO content in mole fraction where the right vertical line represents the axis of symmetry: (**a**) Reactor 1 and (**b**) Reactor 2.

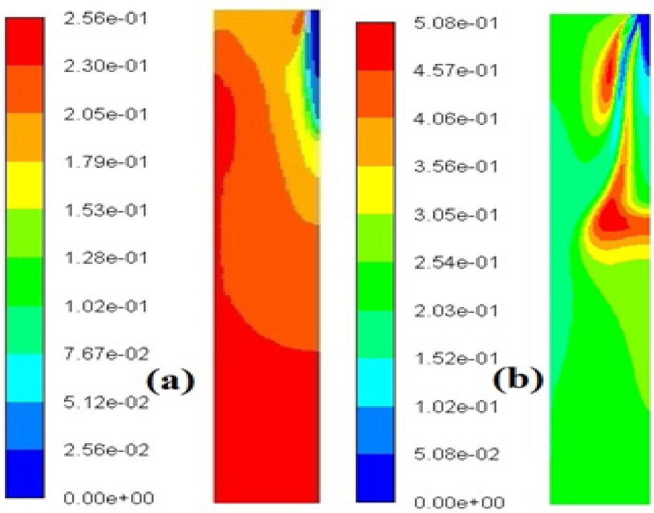

Figure 30. Contours of H_2O vapor content in mole fraction where the right vertical line represents the axis of symmetry: (**a**) Reactor 1 and (**b**) Reactor 2.

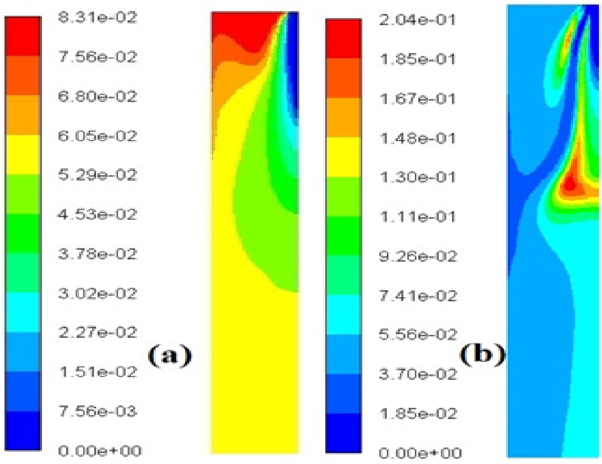

Figure 31. Contours of CO_2 content in mole fraction where the right vertical line represents the axis of symmetry: (**a**) Reactor 1 and (**b**) Reactor 2.

The velocity and temperature distributions in Reactor 1 in Figures 26a and 27a show a single flame where partial oxidation of natural gas produces the reducing gases. The gas mixture expands because of the increase in the temperature and the total molar flow rate of gas products.

Figure 27b shows a split flame which is different from the single flame of Reactor 1 in Figure 27a. The split flame in Reactor 2 arose from the larger thickness of the natural gas stream compared to Reactor 1.

The CO and CO_2 mole fractions in Figures 29 and 31, respectively, show uniform distribution in the last third of the reactors. This differs from the H_2O mole fraction in Figure 30 which shows a uniform distribution in the last fourth of the reactors. These results can be explained from the reduction kinetics as H_2 reacts to a greater extent than CO.

Particle distribution: Particles need to be distributed through the volume of the reactor to increase their reduction. The number density distribution is shown in Figure 32. A higher density near the wall in Reactor 1, which is not favorable, is noticed. A higher density near the walls means that particles are more likely to collide with the wall and stick to the wall. Reactor 2 shows a good distribution of particles and low probability of particles sticking on the wall.

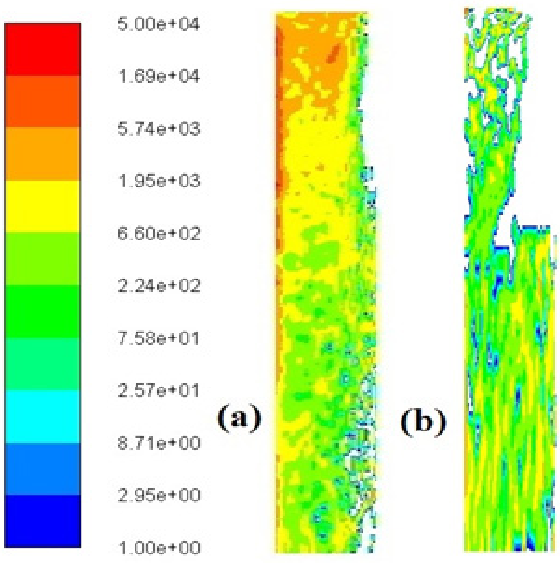

Figure 32. Number density in particles/cm^3 where the right vertical line represents the axis of symmetry: (**a**) Reactor 1 and (**b**) Reactor 2.

The mass weighted average of the mass fraction of metallic iron in particles and the particle temperature profiles are plotted in Figures 33 and 34, respectively, against the axial distance in the reactors starting at the inlet and ending at the outlet of the 35-m long reactor.

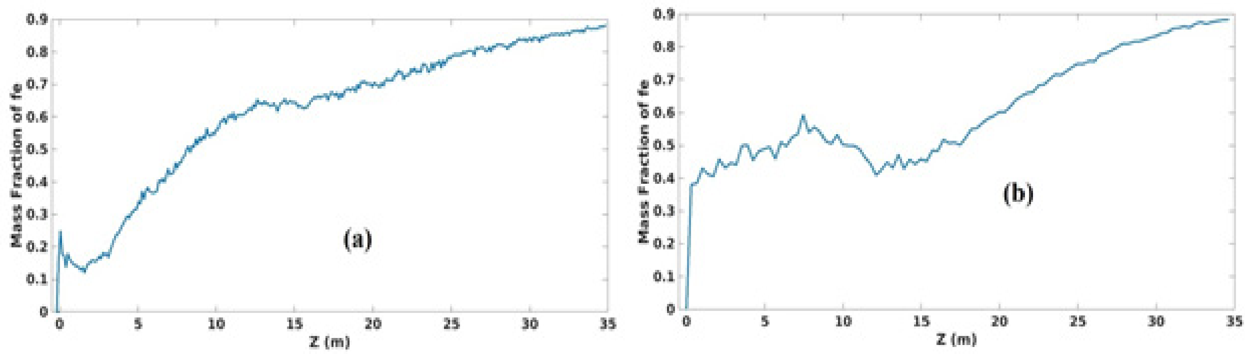

Figure 33. Mass weighted average mass fraction of metallic iron in particles: (**a**) Reactor 1 and (**b**) Reactor 2.

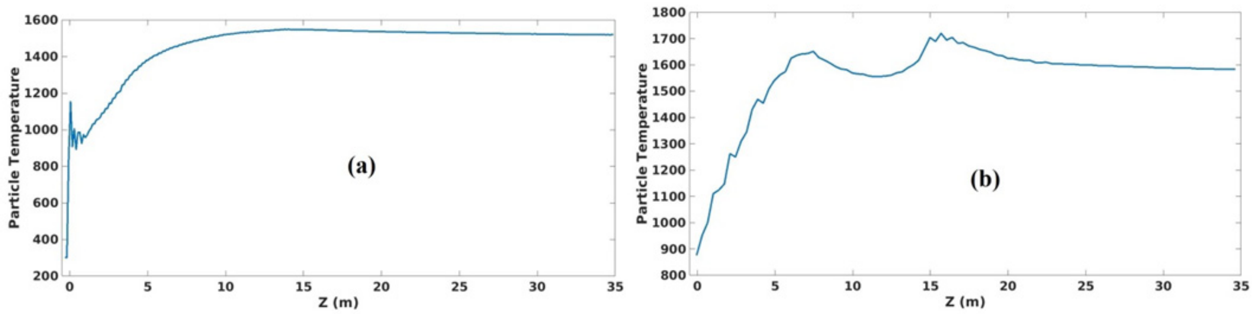

Figure 34. Mass weighted average particle temperature (in K): (**a**) Reactor 1 and (**b**) Reactor 2.

The irregular variations in the curves in Figures 33 and 34 arose from the recirculating flows in the reactors as particles will stay longer on average in those areas. The particle temperature did not reach 1811 K, which is the melting temperature of iron, as we designed the reactor to produce solid iron particles.

Heat loss: The amount of heat generation and the percentage of heat loss in each of the two reactors are summarized in Table 12.

Table 12. Heat generated from the combustion of natural gas, heat loss from the walls, and percentage heat loss.

Reactor	Heat Generated (MW)	Heat Loss (MW)	Percent Heat Loss
1	89.8	1.8	2.0
2	327	3.8	1.2

The numbers indicate that the design of Reactor 2 with a smaller surface area per volume lost only about half of the % heat loss of Reactor 1.

7.4. Summary

Two industrial reactors with different production rates were designed. The metallization degrees of product from these reactors were sufficiently high for use in the subsequent steelmaking step. The modification in Reactor 2 caused higher outlet gas temperature, more uniform temperature along the reactor. Particle distribution showed that Reactor 2 had a better distribution with a lower likelihood of particles sticking on the wall. Reactor 2 also showed a lower percentage of heat loss compared to Reactor 1 because of the lower surface area per volume.

8. Concluding Remarks

Overall, this simulation work has shown that the size of the reactor used in the novel flash ironmaking technology (FIT), even at the production rate comparable to the largest blast furnaces currently used in the steel industry, can be quite reasonable vis-à-vis the blast furnaces. As an example, a flash reactor of 12 m diameter and 35 m with a single burner operating at atmospheric pressure would produce 1.0 million tons of iron per year. The height can be further reduced by using multiple burners or preheating the feed gas. Further, the total volume of the reactor can be greatly reduced by operating the reactor under elevated pressures, from the points of residence time and reaction kinetics. Obviously, the cost of the reactor per unit volume and those of operation and safety measures would increase accordingly. Thus, the actual design will require optimization by taking into consideration these various factors.

The CFD-based design of potential industrial reactors for flash ironmaking pointed to a number of features that an industrial reactor should incorporate. The flow field should be designed in such a way that a larger portion of the reactor is used for the reduction reaction but at the same time excessive collision of particles with the wall must be avoided. Further, a large diameter-to-height ratio that still allows a high reduction degree should be used from the viewpoint of decreased heat loss. This may require the incorporation of multiple burners and solid feeding ports on the reactor roof.

Author Contributions: Conceptualization, H.Y.S., D.-Q.F., and A.A.; software, D.-Q.F.; validation, H.Y.S., D.-Q.F., and A.A.; formal analysis, H.Y.S., D.-Q.F., and A.A.; investigation, H.Y.S., D.-Q.F., and A.A.; resources, H.Y.S.; data curation, D.-Q.F. and A.A.; writing—original draft preparation, H.Y.S., D.-Q.F., and A.A.; writing—review and editing, H.Y.S.; visualization, D.-Q.F. and A.A.; supervision, H.Y.S.; project administration, H.Y.S.; funding acquisition, H.Y.S. All authors have read and agreed to the published version of the manuscript.

Funding: The authors acknowledge the financial support from the U.S. Department of Energy under Award Number DE-EE0005751 with cost share by the American Iron and Steel Institute (AISI) and the University of Utah.

Institutional Review Board Statement: Not applicable.

Informed Consent Statement: Not applicable.

Data Availability Statement: Not applicable.

Acknowledgments: The support and resources from the Center for High Performance Computing at the University of Utah are gratefully acknowledged.

Conflicts of Interest: The authors declare no conflict of interest. The funders had no role in the design of the study; in the collection, analyses, or interpretation of data; in the writing of the manuscript, or in the decision to publish the results.

Disclaimer: This report was prepared as an account of work sponsored by an agency of the United States Government. Neither the United States Government nor any agency thereof, nor any of their employees, makes any warranty, express or implied, or assumes any legal liability or responsibility for the accuracy, completeness, or usefulness of any information, apparatus, product, or process disclosed, or represents that its use would not infringe privately owned rights. Reference herein to any specific commercial product, process, or service by trade name, trademark, manufacturer, or otherwise does not necessarily constitute or imply its endorsement, recommendation, or favoring by the United States Government or any agency thereof. The views and opinions of authors expressed herein do not necessarily state or reflect those of the United States Government or any agency thereof.

References

1. Sohn, H.Y. Suspension Ironmaking Technology with Greatly Reduced Energy Requirement and CO2 Emissions. *Steel Times Int.* **2007**, *31*, 68–72.
2. Tacke, K.-H.; Steffen, R. Hydrogen for the reduction of iron ores- state of the art and future aspects. *Stahl Eisen* **2004**, *124*, 45.
3. IISI. Steel Statistical Yearbook 2007. Available online: http://www.worldsteel.org/pictures/publicationfiles/SSY2007.pdf (accessed on 2017).

4. Lockwood Greene Technologies. *Ironmaking Process Alternatives Screening Study*; Report LG Job No. 010529.01; U.S. Department of Energy: Washington, DC, USA, 2000.
5. Brent, A.D.; Mayfield, P.L.J.; Honeyands, T.A. The Port Hedland FINMET Project–Fluid Bed Production of High Quality Virgin Iron for the 21 "Century". In *International Conference on Alternative Routes of Iron and Steelmaking (ICARISM '99)*; Misra, V.N., Holmes, R.J., Eds.; The Australasian Institute of Mining and Metallurgy: Victoria, Australia, 1999; p. 111.
6. Husain, R.; Sneyd, S.; Weber, P. *Circored and Circofer Two New Fine Ore Reduction Processes. International Conference on Alternative Routes of Iron and Steelmaking (ICARISM '99)*; Misra, V.N., Holmes, R.J., Eds.; The Australasian Institute of Mining and Metallurgy: Victoria, Australia, 1999; p. 123.
7. Macauley, D. Options increase for non-BF ironmaking. *Steel Times Int.* **1997**, *21*, 20.
8. Sohn, H.Y.; Choi, M.E.; Zhang, Y.; Ramos, J.E. Suspension Reduction Technology for Ironmaking with Low CO_2 Emission and Energy Requirement. *Iron Steel Technol.* **2009**, *6*, 158–165.
9. Neelameggham, N.R.; Reddy, R.G.; Belt, C.K.; Vidal, E.E. Energy Technology Perspectives: Carbon Dioxide Reduction and Production from Alternative Sources. In Proceedings of the TMS 2009, San Francisco, CA, USA, 15–19 February 2009; TMS: Warrendale, PA, USA, 2009; pp. 93–101.
10. Sohn, H.Y.; Choi, M.E. Collected Proceedings: Supplemental Proceedings: Vol. 1 Materials Processing and Properties, International Symposium on High-Temperature Metallurgical Processing. In Proceedings of the 139th TMS Annual Meeting, Seattle, WA, USA, 14–18 February 2010; Drelich, J., Hwang, J.-Y., Jiang, T., Downey, J., Eds.; TMS: Warrendale, PA, USA, 2010; pp. 347–354.
11. USGS. *2005 Minerals Yearbook—Iron Ore, (Report, U.S. Department of the Interior)*; U.S. Geological Survey: Reston, VA, USA, 2007.
12. Pinegar, H.K.; Moats, M.S.; Sohn, H.Y. Process Simulation and Economic Feasibility Analysis for a Hydrogen-Based Novel Suspension Ironmaking Technology. *Steel Res. Int.* **2011**, *82*, 951–963. [CrossRef]
13. Pinegar, H.K.; Moats, M.S.; Sohn, H.Y. Flow Sheet Development, Process Simulation and Economic Feasibility Analysis for a Novel Suspension Ironmaking Technology Based on Natural Gas: Part I. Flow Sheet and Simulation for Ironmaking with Reformerless Natural Gas. *Ironmak. Steelmak.* **2012**, *39*, 398–408. [CrossRef]
14. Pinegar, H.K.; Moats, M.S.; Sohn, H.Y. Flow Sheet Development, Process Simulation and Economic Feasibility Analysis for a Novel Suspension Ironmaking Technology Based on Natural Gas: Part II. Flow Sheets and Simulation for Ironmaking Combined with Steam-Methane Reforming. *Ironmak. Steelmak.* **2013**, *40*, 32–43. [CrossRef]
15. Pinegar, H.K.; Moats, M.S.; Sohn, H.Y. Flow Sheet Development, Process Simulation and Economic Feasibility Analysis for a Novel Suspension Ironmaking Technology Based on Natural Gas: Part III: Economic Feasibility Analysis. *Ironmak. Steelmak.* **2013**, *40*, 44–49. [CrossRef]
16. Fan, D.-Q.; Mohassab, Y.; Elzohiery, M.; Sohn, H.Y. Analysis of the Hydrogen Reduction Rate of Magnetite Concentrate Particles in a Drop Tube Reactor Through CFD Modeling. *Met. Mater. Trans. B* **2016**, *47B*, 1669–1680. [CrossRef]
17. Fan, D.-Q.; Elzohiery, M.; Mohassab, Y.; Sohn, H.Y. Rate-Enhancement Effect of CO in Magnetite Concentrate Particle Reduction by H_2+CO Mixtures. *Ironmak. Steelmak.* under review.
18. Fan, D.-Q.; Sohn, H.Y.; Elzohiery, M. Analysis of the Reduction Rate of Hematite Concentrate Particles by H2 or CO in a Drop-Tube Reactor through CFD Modeling. *Met. Mater. Trans. B* **2017**, *48B*, 2677–2684. [CrossRef]
19. Elzohiery, M.; Sohn, H.Y.; Mohassab, Y. Kinetics of Hydrogen Reduction of Magnetite Concentrate Particles in Solid State Relevant to Flash Ironmaking. *Steel Res. Int.* **2016**, *88*. [CrossRef]
20. Elzohiery, M.; Fan, D.; Mohassab, Y.; Sohn, H.Y. Kinetics of hydrogen reduction of magnetite concentrate particles at 1623–1873 K relevant to flash ironmaking. *Ironmak. Steelmak.* **2020**, 1–8. [CrossRef]
21. Fan, D.-Q.; Elzohiery, M.; Mohassab, Y.; Sohn, H.Y. The kinetics of carbon monoxide reduction of magnetite concentrate particles through CFD modelling. *Ironmak. Steelmak.* **2021**, 1–10. [CrossRef]
22. Wang, H.; Sohn, H.Y. Effects of Reducing Gas on Swelling and Iron Whisker Formation during the Reduction of Iron Oxide Compact. *Steel Res. Int.* **2012**, *83*, 903–909. [CrossRef]
23. Chen, F.; Mohassab, Y.; Jiang, T.; Sohn, H.Y. Hydrogen Reduction Kinetics of Hematite Concentrate Particles Relevant to a Novel Flash Ironmaking Process. *Met. Mater. Trans. A* **2015**, *46*, 1133–1145. [CrossRef]
24. Chen, F.; Mohassab-Ahmed, M.Y.; Zhang, S.; Sohn, H.Y. Kinetics of the Reduction of Hematite Concentrate Particles by Carbon Monoxide Relevant to a Novel Flash Ironmaking Process. *Met. Mater. Trans. A* **2015**, *46*, 1716–1728. [CrossRef]
25. Fan, D.-Q.; Sohn, H.Y.; Mohassab, Y.; Elzohiery, M. Computational Fluid Dynamics Simulation of the Hydrogen Reduction of Magnetite Concentrate in a Laboratory Flash Reactor. *Met. Mater. Trans. A* **2016**, *47*, 3489–3500. [CrossRef]
26. Elzohiery, M.; Fan, D.; Mohassab, Y.; Sohn, H.Y. Experimental Investigation and Computational Fluid Dynamics Simulation of the Magnetite Concentrate Reduction Using Methane-Oxygen Flame in a Laboratory Flash Reactor. *Met. Mater. Trans. A* **2020**, *51*, 1003–1015. [CrossRef]
27. Elzohiery, M. Flash Reduction of Magnetite Concentrate Related to a Novel Flash Ironmaking Process. Ph.D. Dissertation, University of Utah, Salt Lake City, UT, USA, 2018.
28. Fan, D.-Q. Computational Fluid Dynamics analysis and Design of Flash Ironmaking Reactors. Ph.D. Dissertation, University of Utah, Salt Lake City, UT, USA, 2019.
29. Abdelghany, A.; Fan, D.-Q.; Elzohiery, M.; Sohn, H.Y. Experimental Investigation and Computational Fluid Dynamics Simulation of a Novel Flash Ironmaking Process Based on Partial Combustion of Natural Gas in a Reactor. *Steel Res. Int.* **2019**, *90*. [CrossRef]
30. Jones, W.P.; Lindstedt, R.P. Global reaction schemes for hydrocarbon combustion. *Combust. Flame* **1988**, *73*, 233–249. [CrossRef]